



## Research article

# The multi-omics analysis identifies a novel cuproptosis-anoikis-related gene signature in prognosis and immune infiltration characterization of lung adenocarcinoma

Guanyu Jiang<sup>a,1</sup>, Chenghu Song<sup>a,1</sup>, Xiaokun Wang<sup>a,1</sup>, Yongrui Xu<sup>a</sup>, Huixing Li<sup>a</sup>, Zhao He<sup>a</sup>, Ying Cai<sup>b,\*\*\*</sup>, Mingfeng Zheng<sup>a,\*\*</sup>, Wenjun Mao<sup>a,\*</sup>

<sup>a</sup> Department of Thoracic Surgery, The Affiliated Wuxi People's Hospital of Nanjing Medical University, Wuxi, 214023, China

<sup>b</sup> Department of Pathology, The Affiliated Wuxi People's Hospital of Nanjing Medical University, Wuxi, 214023, China



## ARTICLE INFO

## Keywords:

TCGA  
Anoikis  
Cuproptosis  
Lung adenocarcinoma  
Immune infiltration

## ABSTRACT

**Background:** Lung adenocarcinoma (LUAD) has emerged as one of the most aggressive lethal cancers. Anoikis serves as programmed apoptosis initiated by the detachment of cells from the extracellular matrix. Cuproptosis is distinct from traditional cell death modalities. The above two modes are both closely related to tumor progression, prognosis, and treatment. However, whether they have synergistic effects in LUAD deserves further investigation.

**Methods:** The anoikis-related prognostic genes (ANRGs) co-expressed with cuproptosis-associated genes (CAGs) were screened using correlation analysis, analysis of variance, least absolute shrinkage, and selection operator (LASSO), and COX regression followed by functional analysis, and then LUAD risk score model was constructed. Using consensus clustering, the relationship between different subtypes and clinicopathological features, immune infiltration characteristics, and somatic mutations was analyzed. A nomogram was developed by incorporating clinical information, which provided a prediction of the survival of patients. Finally, a comprehensive analysis of ANRGs was performed and verified by the HPA database.

**Results:** A total of 27 ANRGs associated with cuproptosis were obtained. On this basis, three distinct ANRGs subtypes were identified, and the differences between clinical prognosis and immune infiltration were observed. A risk score model has been constructed by incorporating seven ANRGs signatures (EIF2AK3, IKZF3, ITGAV, OGT, PLK1, TRAF2, XRCC5). A highly reliable nomogram was developed to help formulate treatment strategies based on risk score and the clinicopathological features of LUAD. The seven-gene signature was turned out to be strongly linked to immune cells and validated in single-cell data. Immunohistochemistry proved that all of them are highly expressed in LUAD tissues.

**Conclusion:** This study reveals the potential relationship between cuproptosis-related ANRGs and clinicopathological features, tumor microenvironment (TME), and mutation characteristics, which can be applied for predicting the prognosis of LUAD and help develop individualized treatment strategies.

\* Corresponding author.

\*\* Corresponding author.

\*\*\* Corresponding author.

E-mail addresses: [jianggy2021@stu.njmu.edu.cn](mailto:jianggy2021@stu.njmu.edu.cn) (G. Jiang), [cy3163@163.com](mailto:cy3163@163.com) (Y. Cai), [zhengmfmedical@126.com](mailto:zhengmfmedical@126.com) (M. Zheng), [maowenjun1@njmu.edu.cn](mailto:maowenjun1@njmu.edu.cn) (W. Mao).

<sup>1</sup> These authors have contributed equally to this work and share first authorship.

<https://doi.org/10.1016/j.heliyon.2023.e14091>

Received 16 November 2022; Received in revised form 18 February 2023; Accepted 22 February 2023

Available online 27 February 2023

2405-8440/© 2023 The Authors. Published by Elsevier Ltd. This is an open access article under the CC BY-NC-ND license (<http://creativecommons.org/licenses/by-nc-nd/4.0/>).

## 1. Introduction

LUAD is among the most highly invasive and lethal cancer types in the world with a very low five-year survival rate (<20%) [1,2]. Currently, the primary treatment modalities for LUAD comprise surgery, radiation, and chemotherapy, as well as targeted therapy and immunotherapy [3]. There is still a lack of suitable treatment options for many LUAD patients despite the increasing number of novel treatments being introduced into clinical practice. Considering LUAD's high mutagenicity and metastatic nature, developing an effective gene signature to reveal the potential mechanism of tumor metastasis is critical for predicting patient prognosis and guiding clinical treatment.

Anoikis refers to one kind of programmed cell death induced by normal adherent cells disconnected from the extracellular matrix (ECM) for a long time, which is indispensable for maintaining tissue stability and preventing abnormal cell growth or cell adhesion to abnormal ECM [4]. After detaching from the adhesion of ECM and cell-to-cell contact, tumor cells can survive through autocrine and paracrine mechanisms and resist anoikis, regaining the adhesion ability to metastasize and invade [5]. Therefore, further study on the molecular mechanism of controlling anti-anoikis in tumors can help explore better therapeutic directions.

Copper is a key cofactor for all life forms. Copper ion carriers are small molecules that bind to copper and transport it into cells. Several pieces of evidence suggest that the mechanism of copper ion carrier-induced cell death involves the accumulation of intracellular copper [6]. Tsvetkov et al. have demonstrated that copper ion carrier-induced cell death could be a new cell death pathway, which is quite distinct from traditional cell death modalities such as necroptosis, ferroptosis, etc. This process is called cuproptosis. The researchers found that copper ions cause abnormal aggregation of thioredoxin by directly binding to thioredoxin in the tricarboxylic acid cycle and interfering with iron-sulfur proteins (Fe/S protein) in the respiratory chain complex, resulting in a proteotoxic stress response that ultimately leads to cell death [7].

Significant change of copper ion level would occur in tumor tissue. These variations may enhance the development or aggressiveness of the tumor [8]. Cuproptosis requires the participation of mitochondrial respiration and significantly reduces the respiratory reserve capacity [9]. When copper overload occurs, it disrupts the iron-sulfur cofactor and stimulates the copper-driven Fenton reaction and generates destructive ROS [6]. Reactive oxygen species (ROS) serve as highly active state of oxygen, produced in the process of mitochondrial oxidative metabolism, including cardiovascular disease, cancer and autoimmune disorders [10]. ROS can stimulate glucose oxidation and enhances oxidative stress in cancer cells, restoring cellular susceptibility to anoikis [11]. XIAP, a key molecule in cell death, is involved in the regulation of neuronal differentiation, intracellular ROS production and copper homeostasis. XIAP could regulate MURR1 protein reduction through ubiquitination and proteasomal degradation, thus regulating intracellular copper levels, might participate in the process of cuproptosis [12]. After cytochrome c promoting the activation of caspase9, XIAP, as an important regulator of the balance between cell survival and cell death, can bind to caspase9, and then induced anoikis [13]. Studies have shown that Tetrathiomolybdate (TM) could significantly enhance the anoikis of tumor cells by down-regulating XIAP protein [14]. In contrast, the synergistic effect of cuproptosis and anoikis in tumor progression as well as metastasis has not been thoroughly explored further. Herein, the relationship between cuproptosis co-expressed anoikis-related genes (ANRGs) and various LUAD subtypes, mutation characteristics, and tumor microenvironment (TME) have been comprehensively evaluated and constructed an ANRGs-based risk scoring model which could help to develop therapeutic options that are more individualized and accurate.

## 2. Materials and methods

### 2.1. Data collection and cohorts processing

Transcriptome data of lung cancer (TCGA-LUAD) along with associated clinical and somatic mutation data were accessed from The Cancer Genome Atlas (TCGA; <https://portal.gdc.cancer.gov/>) database. The copy number variant data have been captured utilizing the UCSC Xena [15] (<https://xena.ucsc.edu/>) database. In turn, the LUAD dataset GSE26939 was acquired from Gene Expression Omnibus (GEO; <https://www.ncbi.nlm.nih.gov/geo/>). The FPKM values of TCGA-LUAD were translated into transcripts per kilobase million (TPM) identical to those from microarrays. The two datasets were combined, and the batch effect of merged cohort was removed by using the R package "SVA". The final dataset (TCGA-GEO) contained 632 LUAD clinical features like age, sex, tumor, node, metastasis, stage, survival status, and follow-up time have been involved.

### 2.2. Acquisition of anoikis-related prognostic genes co-expressed with cuproptosis

A total of 13 genes related to cuproptosis have been identified referring to a previous study [7], followed by acquisition of 557 genes related to anoikis utilizing the GeneCards (<https://www.genecards.org/>) database and Harmonizome portals [16]. The R package "limma" was applied to calculate the anoikis-related genes whose expressions were positively correlated with cuproptosis-associated genes ( $\text{cor} > 0.3$ ). For constructing the Venn diagram, these anoikis-related genes were intersected with genes in TCGA-GEO data set by the jvenn portal (<http://jvenn.toulouse.inra.fr/app/index.html>) [17], and also compared their expressions in normal and tumor tissues to obtain significantly different genes. Univariate Cox regression was performed on differentially expressed genes (DEGs) to obtain the final prognosis-related genes, and then the forest map was plotted.

### 2.3. Characterization analysis of anoikis-related prognostic genes (ANRGs)

The interactions among ANRGs have been examined while analyzing their somatic mutation incidence, genetic loci, and CNV. For ANRGs, the protein-protein interaction network (PPI) has been generated from the STRING (<https://cn.string-db.org/>) database [18]. Finally, GO [19] as well as KEGG [20] functional analyses were performed using the R package “ClusterProfiler”.

### 2.4. Consensus clustering analysis of ANRGs

Consistent unsupervised clustering analysis was performed by using R package “ConsensusClusterPlus”, thereby patients were divided into different molecular subtypes based on ANRG expression. On this basis, the reliability of clustering was verified by principal component analysis (PCA) utilizing the “ggplot2” package. After this, the intra-group and inter-group correlations increased and decreased respectively. The differential analysis of ANRG expression across different subtypes has been performed and then compared the prognostic value of patients with different subtypes by R package “ClusterSur”.

### 2.5. Molecular subtyping and clinical immune characterization of ANRGs

The relationship among molecular subtypes, clinicopathological features (including age, sex, tumor, node, metastasis, and stage), and prognosis were analyzed, which showed disparate clinical value of different subtypes identified by the consensus clustering method. Subsequently, single sample gene set enrichment analysis (ssGSEA) was applied to assess the relationship between different subtypes and immune cell infiltration. The enrichment analyses have been carried out utilizing the MSigDB database’s ‘c2.cp.kegg.v7.5.1.symbols.gmt’ data and the ‘GSVA’ R package.

### 2.6. Development of the ANRG-based risk-scoring model

All samples were equally classified into the training (n = 311) and test groups (n = 311) to develop the risk score model of ANRGs prognostic signatures. The “glmnet” R package was utilized for minimizing the risks of over-fitting by applying the Lasso COX regression algorithm on ANRGs. The changing trajectory for every independent variable has been examined and then subjected to 10-fold cross-validation to build a model. Multivariate Cox analysis has been done to select candidate genes to establish a risk score of the ANRGs signature in the training set.

The risk score of the ANRGs signature was depicted as followed:

$\text{RiskScore} = \sum (\text{Expi} * \text{coefi})$ , Coefi and Expi denoting the risk coefficient and expression for each gene. Based on the median risk score, the training cohort was classified into low-risk group and high-risk group, and Kaplan-Meier (KM) survival analysis was performed subsequently. Similarly, the testing and all sets have been classified into low-as well as high-risk groups. KM survival curves as well as receiver operational feature curves (ROCs) were applied to assess the model’s predictive ability.

### 2.7. Construction and characteristics of nomogram for risk scoring model

Final nomogram was established with R package “rms” according to the clinicopathological features and risk score. Its clinical reliability has been verified by analyzing the calibration curve. Forest plot was applied to instantiate the influence of each variable on the model (p-values, HR, and 95% CI). Decision curve analysis (DCA) was used to evaluate the net benefit value of model under different thresholds.

### 2.8. Stratification analysis based on risk score

The differences in risk scores were compared by cluster typing, while CIBERSORT was used for evaluating the proportion of immune cell types across low-as well as high-risk groups, with the sum of all estimated immune cell type scores in each sample being 1. At the same time, spearman rank correlation was used to test the relationship between risk score and immune cell infiltration. Further, the relationships between the two risk groups and the tumor microenvironment score, tumor mutational burden, microsatellite instability (MSI), and tumor stem cell (CSC) index were also analyzed.

### 2.9. Comprehensive analysis of risk score-associated prognostic markers

The relationship between 22 infiltrating immune cell components and risk score prognostic signatures has been explored. Then “MAF Tools” (R package) were applied to analyze somatic mutation patterns based on risk groups. Further, the correlation between ANRGs and the chemosensitivity of various small molecule drugs in the GDSC and CTRP databases by Gene Set Cancer Analysis (GSCA; <http://bioinfo.life.hust.edu.cn/GSCA/#/>) database [21] has also been examined. Tumor Immune Single-Cell Hub (TISCH; <http://tisch.comp-genomics.org/>) [22], a large single-cell RNA-SEQ online database focused on TME has been applied for the systematic study of TME heterogeneity across different datasets as well as cell types. The LUAD single-cell dataset GSE146100 was selected for further analyzing the immune profiles of markers. In the Human Protein Atlas (HPA; <https://www.proteinatlas.org/>), human proteins are mapped in organs, tissues, and cells by combining omics techniques, and this dataset was applied to obtain immunohistochemical images of individual marker proteins in LUAD.

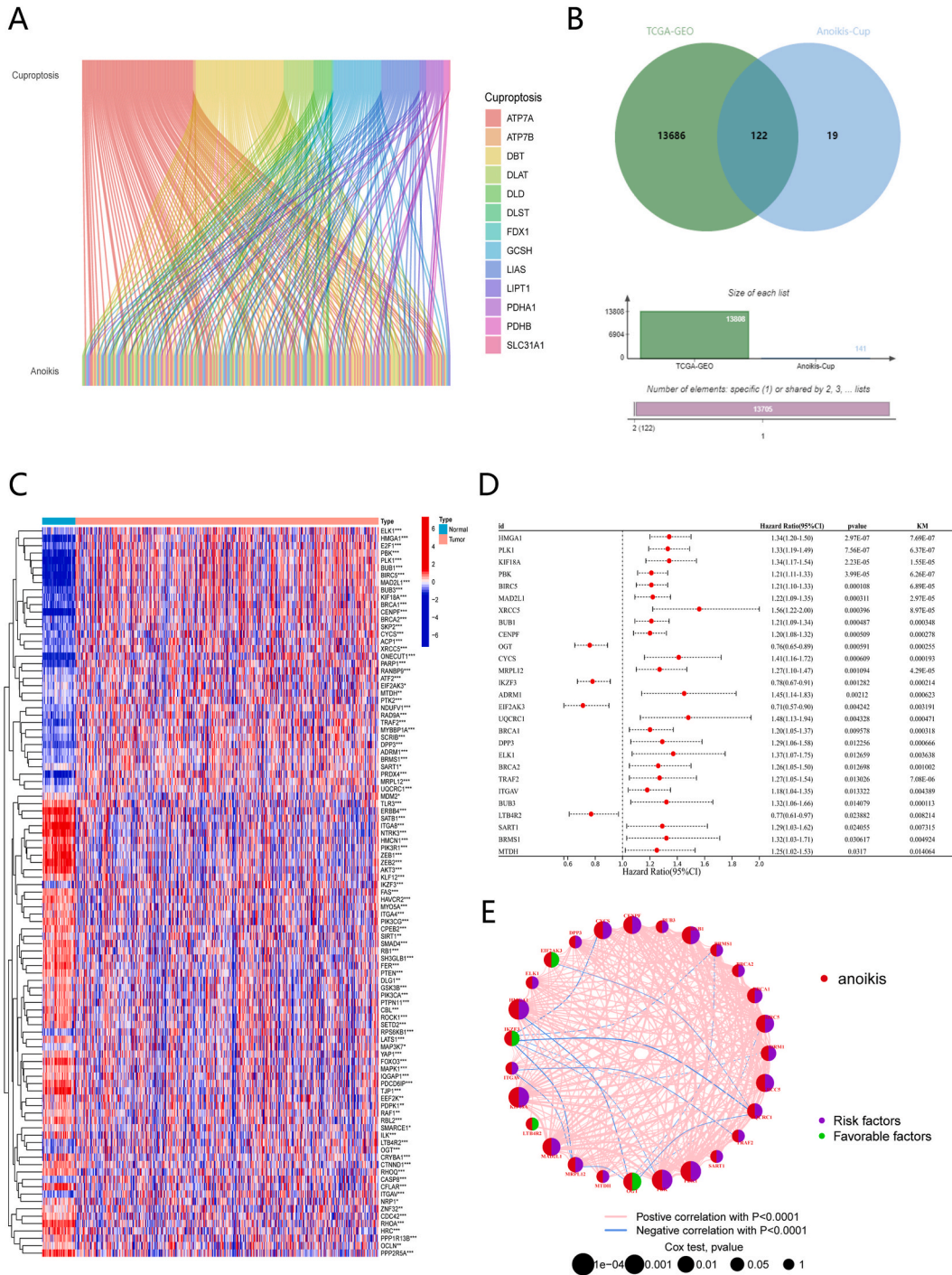


**Fig. 1.** Identifying cuproptosis co-expressed anoikis-related prognostic genes (ANRGs) in LUAD. (A) Sankey diagram showing the positive correlation between 13 cuproptosis-associated genes and 141 anoikis-related genes ( $cor > 0.3$ ). (B) Identification of 122 intersecting genes by Venn chart. (C) Heat map revealing the differentially expressed ANRGs between tumor and normal tissue. (D) A forest plot illustrating 27 ANRGs obtained by univariate COX regression analysis. (E) The interaction network of 27 ANRGs in LUAD. The differences in correlations are indicated by different colors. (For interpretation of the references to color in this figure legend, the reader is referred to the Web version of this article.)

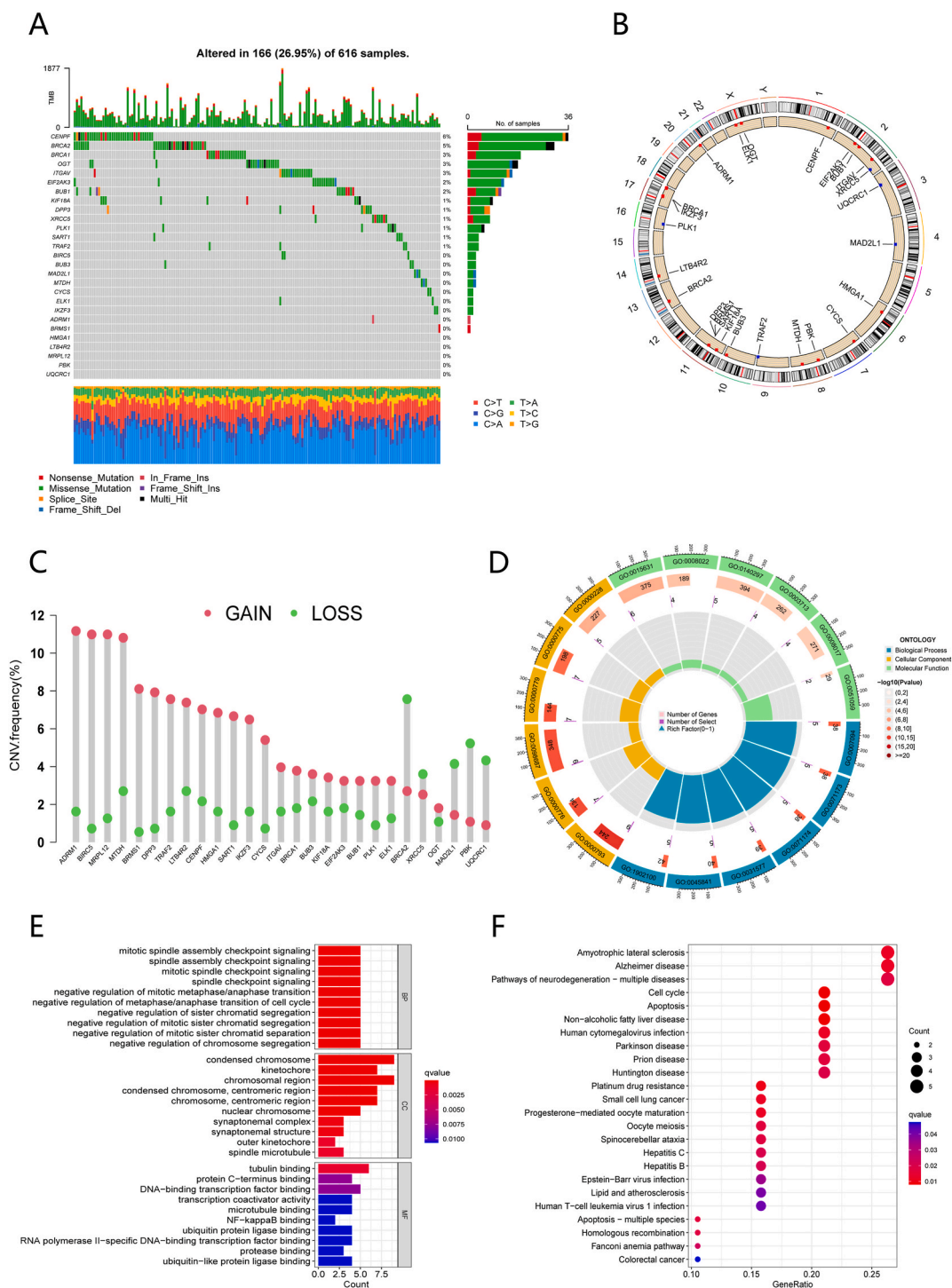
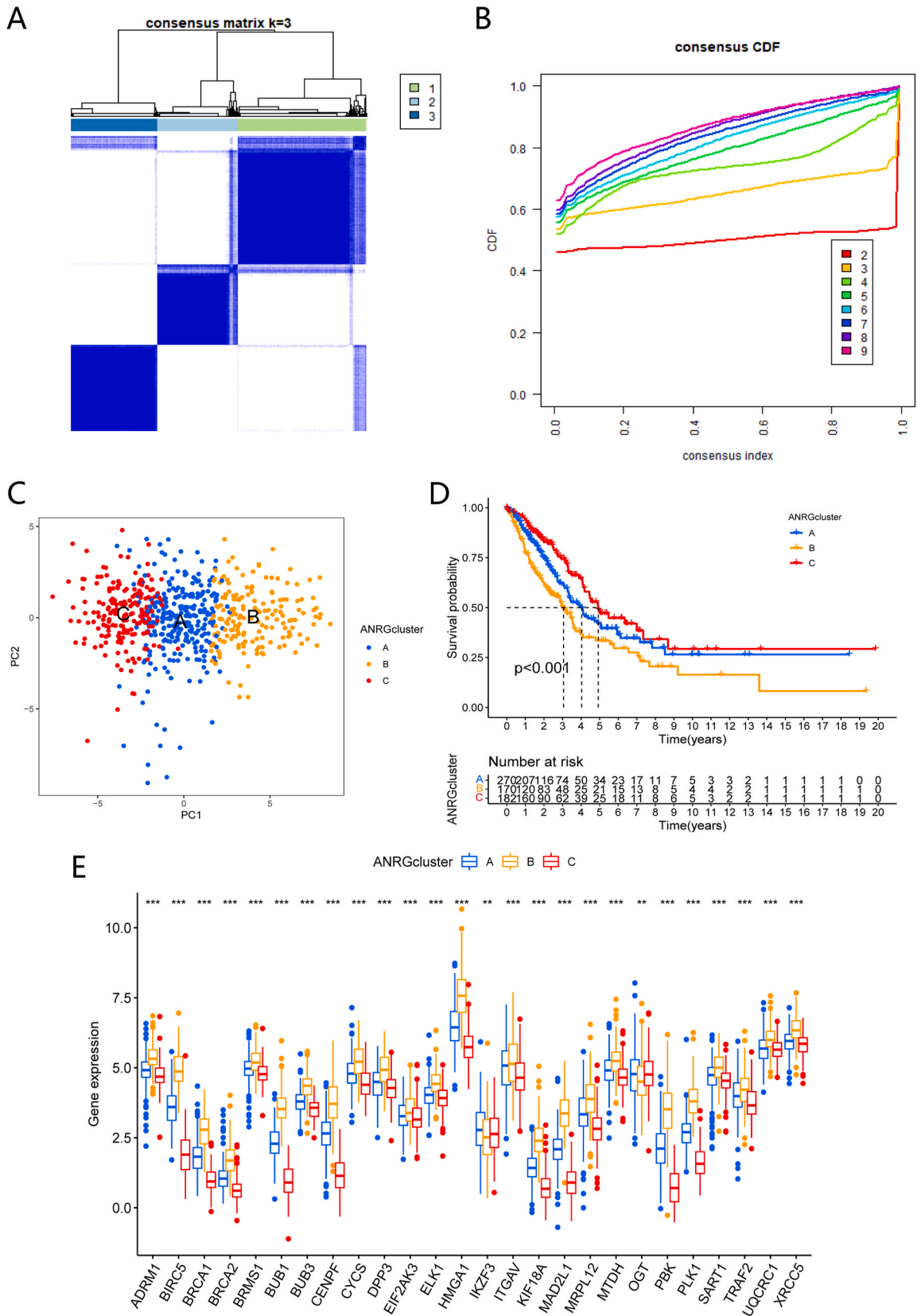


**Fig. 2.** The landscape of mutation characteristics and function of ANRGs. (A) Mutation profiles of 27 ANRGs in 616 samples. The right bar chart illustrates the frequency of mutations, and the stacked bar chart below depicts various mutation types. (B) The alteration localization of ANRGs on 23 chromosomes. (C) CNVs frequency of 27 ANRGs in LUAD. (D-E) Circle chart and bar plot for GO analyses of ANRGs. (F) Bubble plot illustrating KEGG pathway enrichment analyses.



(caption on next page)

**Fig. 3.** Subtypes of LUAD based on ANRGs. (A) Consensus clustering matrix defining three subtypes with  $k = 3$ . (B) The cumulative distribution function (CDF) plot shows the fractal reliability when  $k$  takes different values. (C) PCA shows remarkable differences across the three subtypes based on ANRGs expression. (D) K-M curve showing significant OS differences between the three clusters. (E) Analysis of differential ANRGs expression in various subtypes.

### 2.10. Statistical analysis

Statistical differences between two groups were compared by Wilcoxon test, while differences among three groups were compared using the Kruskal-Wallis test or ANOVA. Analysis of correlation coefficients was conducted using Spearman's correlation coefficient, while the independent predictors of OS were determined by univariate and multivariate Cox regression analyses. A two-sided P value of less than 0.05 was considered statistically significant (\* $P < 0.05$ , \*\* $P < 0.01$ , and \*\*\* $P < 0.001$ ). All statistical analyses and drawings were conducted by R software version 4.2.1.

## 3. Results

### 3.1. Identifying cuproptosis co-expressed anoikis-related prognostic genes

The whole 141 anoikis-associated genes were discovered to be positively co-expressed ( $\text{cor} > 0.3$ ) with cuproptosis-associated genes after calculations (Fig. 1A, Supplementary Table S1). Then, 122 common genes were acquired by Venn Plot (Fig. 1B), and for verifying their role in LUAD, their expression between tumor and normal tissues has been compared. LUAD tissues exhibited significant upregulation of 43 genes among those DEGs (Fig. 1C). As shown in Figs. S1 and S2, 27 out of 43 DEGs were significantly associated with prognosis as per a univariate COX regression analysis. According to the forest plot (Figs. 1D), 23 genes, excluding OGT, IKZF3, EIF2AK3, and LTB4R2, were found to be linked to poor prognosis. A network diagram of 27 ANRGs was constructed, which comprehensively analyzed the interrelationship among these genes as well as their influence on LUAD patients' prognoses (Fig. 1E).

### 3.2. Genetic variation and functional analysis of ANRGs

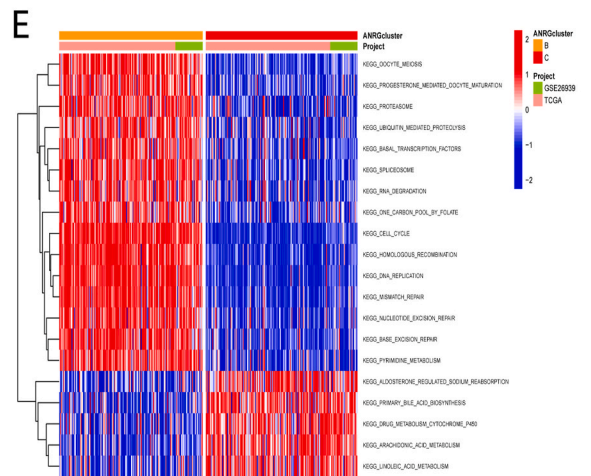
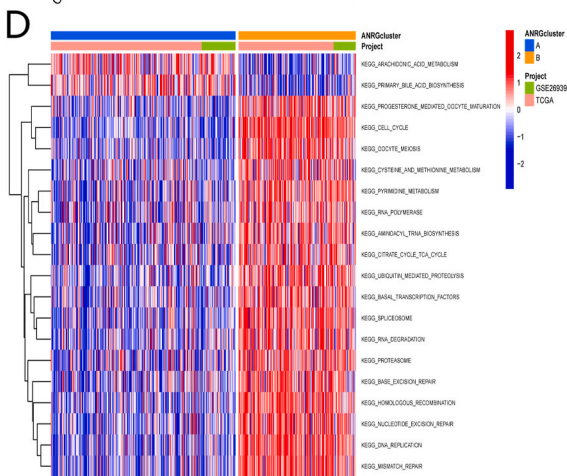
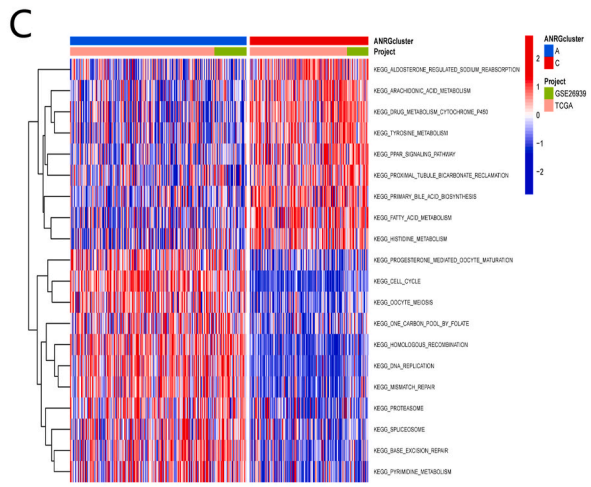
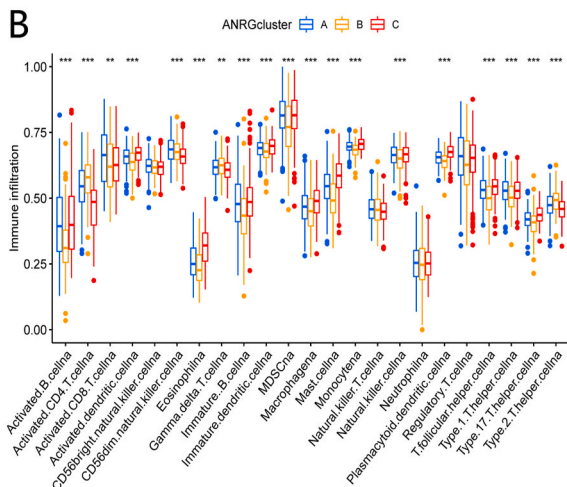
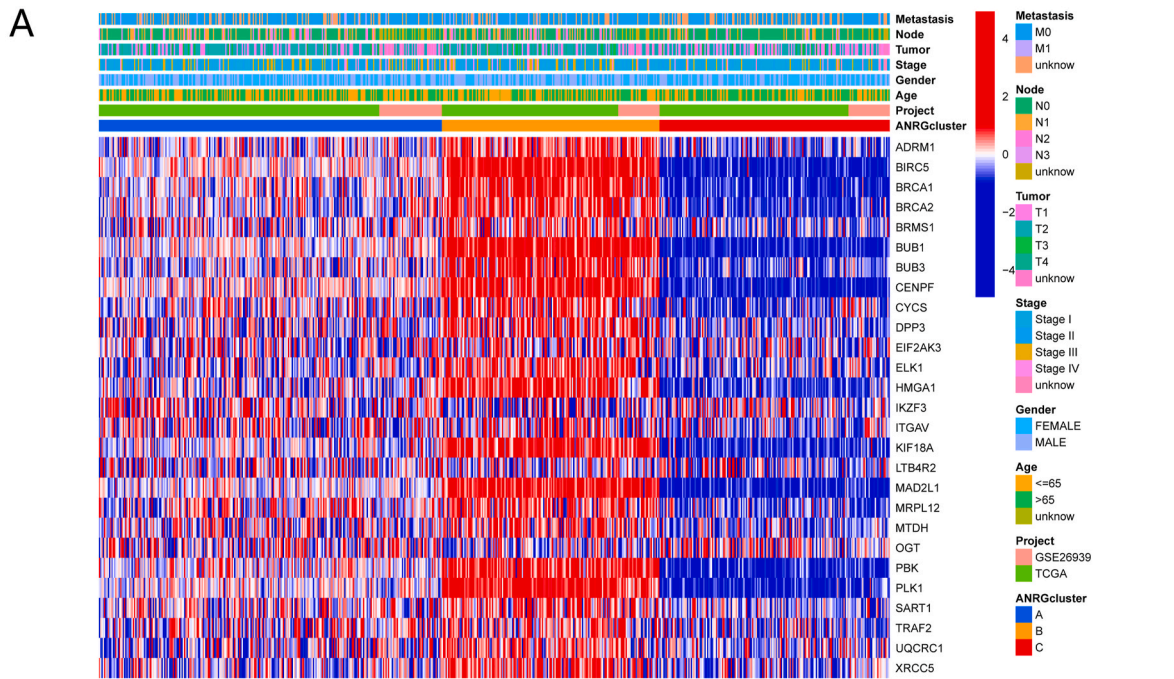
As illustrated in Fig. 2A, the somatic mutation status of ANRGs in LUAD has been evaluated, which revealed that 166 (26.95%) of 616 LUAD samples had mutations with the CENPF gene possessing the highest mutation rate, followed by BRCA2 and BRCA1. The five ANRGs (HMGA1, LTB4R2, MRPL12, PBK, and UQCRC1) were not mutated. The interactions between ANRGs, as revealed by PPI analysis, are depicted in Fig. S3. Moreover, exploring the somatic CNV of these ANRGs showed their prevalence in all 27 ANRGs. Among these, ADRM1, BIRC5, MRPL12, and MTDH had extensively increased CNV while BRCA2, XRCC5, MAD2L1, PBK, and UQCRC1 had moderately decreased CNV (Fig. 2B). Fig. 2C depicted CNV alterations on the ANRGs' respective chromosomes. To explore the potential biological behavior of ANRGs, a functional enrichment analysis of 27 genes was conducted. GO showed that these genes were mainly linked to mitosis and cell cycle regulation (Fig. 2D–E). KEGG analysis proved that they were significantly concentrated in apoptosis, cell cycle, and neurodegenerative pathways (Fig. 2F).

### 3.3. Consistent clustering typing analysis based on ANRGs in LUAD

To investigate the ANRGs' clinical significance and functional biological patterns, consensus clustering has been conducted for categorizing LUAD patients as per ANRGs' expression levels. Fig. 3A–B shows that the whole cohort was well separated into subtypes A, B, and C when  $K = 3$ . Furthermore, based on ANRGs expression, PCA showed considerable variations in the transcriptional profiles of ANRGs across three subtypes (Fig. 3C). Moreover, remarkable variations were detected in the Kaplan-Meier survival curves of the three subgroups, with patients in cluster B having the worst prognosis (Fig. 3D). The box plot showed considerable variations in ANRG expression among three subtypes, except for IKZF3 and OGT, other genes' expressions were remarkably higher in cluster B than that in clusters A or C which further demonstrated that ANRGs play a key role in determining prognoses for LUAD patients and may serve as potential therapeutic targets (Fig. 3E).

### 3.4. Clinical characterization and immune infiltration analysis of genotyping

A comparison of clinicopathological characteristics of various LUAD subtypes indicated significant differences (Fig. 4A). Further, to determine the relationship between ANRGs and TME, the infiltration degree of 23 immune cells in three subtypes was evaluated by using ssGSEA analysis. As shown in Fig. 4B, significant discrepancies in the enrichment of major immune cells were observed between these clusters. The expression of other immune cells was lowest in cluster B, except activated  $\text{CD4}^+$  T-cells, Gamma delta ( $\gamma\delta$  T cells) T-cells, and Type-2 T-helper-cells (TH2). The cluster B was significantly concentrated in the TCA cycle, DNA replication mismatch repair, nucleotide excision repair, base-excision repair, homologous recombination, and other cell cycle-related functions as revealed by the GSVA enrichment analysis. On the other hand, cluster C was significantly concentrated in metabolic pathways including arachidonic-acid-metabolism, Tyrosine metabolism, Fatty Acid Metabolism, Histidine metabolism and the PPAR signaling pathway (Fig. 4C–E).



(caption on next page)

**Fig. 4.** Clinical characterization and immune infiltration analysis in three subtypes of LUAD. (A) Differences in ANRG expression and respective clinicopathological features across the three different clusters as depicted in a heat map. (B) Profiles in immune infiltration among three clusters. (C–E) GSVA of biological processes across the three independent subtypes with red representing activated pathways and blue representing inhibited pathways. (For interpretation of the references to color in this figure legend, the reader is referred to the Web version of this article.)

### 3.5. Construction of ANRGs risk model

To exploit the value of ANRGs in LUAD clinical treatment, the above genes were utilized to establish a prognostic model capable of quantifying each patient's prognosis by applying a minimal  $\lambda$  Lasso-Cox regression analysis for further selecting the best prognostic indicator (Fig. 5A–B) and finally obtained a risk score model “ANRGsScore” integrating seven ANRGs markers. In accordance with the multivariate COX result, the following formula was established: Risk Score =  $(-0.5208 * EIF2AK3) + (-0.2569 * IKZF3) + (0.1752 * ITGAV) + (-0.3677 * OGT) + (0.1646 * PLK1) + (0.3154 * TRAF2) + (0.4500 * XRCC5)$ . Seven hub ANRGs expression patterns (Fig. 5C–D), risk score distributions, and clinical status of patients across both low- as well as high-risk subgroups have been compared for two cohorts: the training (n = 311) and testing sets (n = 311). The ROC curves were plotted over time to calculate the area under the ROC curve (AUC) at different time points to estimate the performance of the prediction model. The risk distribution plots showed that with increasing risk score, survival time decreased, while mortality increased (Fig. 5E–H). In the training set, the AUC for 1-, 3-, and 5-year survival was correspondingly 0.732, 0.743, and 0.712, respectively (Fig. 6A). The validation set also likewise indicated that the model was instructive for clinical applications (Fig. 6B). In the high-risk subgroup, K-M survival analyses of both sets showed a worse prognosis (Fig. 6C–D).

### 3.6. Risk score-based nomogram

For quantifying the individual risk assessment of LUAD patients while taking into account the impact of clinicopathological and other factors on the prognosis model, a nomogram containing ANRGs Score and clinical information has been constructed for anticipating 1-, 3-, and 5-year survival probability. The nomogram primarily included three parameters, that is, T- and N-stage along with ANRGs Score (Fig. 6E). DCA was used to determine the usability and effectiveness of the prediction model, which proved that the nomogram could predict the survival probability of LUAD patients at different times (Fig. 6F). Further, the calibration chart demonstrated that the developed nomogram performed similarly to the ideal model (Fig. 6G). The forest plot also further demonstrated that T Stage, N Stage, and ANRGs Score in nomogram were the main factors affecting prognosis (Fig. 6H). The relationship across the three subtypes, risk scores, and clinical outcomes of cluster B patients was identified in Sanger diagrams for visualizing their clinical characteristics, and we found that most of the cluster B patients with high-risk scores have died which was also consistent with previous conclusions.

### 3.7. Correlation analysis between different risk scores, tumor microenvironment, and mutation characteristics

Three subtypes of LUAD showed considerable variations in their respective risk scores when analyzing the link between risk score and subtypes of LUAD (Fig. 7A). For the immune infiltration difference of the tumor microenvironment among different risk scores, the correlation of different immune cells provided clues for the composition of the immune microenvironment (Fig. 7B). Significant variations of immune cell infiltration could be found in the comparison between the high-risk and low-risk groups (Fig. 7C). The low-risk group showed superior infiltration of immune cells involved in tumor immune activation, such as B cells memory, T cells CD4 memory resting, monocytes, and mast cells resting (Fig. 7C). In addition, the tumor microenvironment mesenchymal and immune score in various risk groups was also obtained (Fig. 7D). In previous studies, TMB and MSI have been linked to immunotherapy effects. Interestingly, compared to the low-risk group, mutation data analysis showed significantly higher TMB in the high-risk group (Fig. 7E), implying it may benefit from immunotherapy. Correlation analysis revealed that the ANRGs Score was positively associated with TMB across different subtypes (Fig. 7F). In terms of MSI, a low ANRGs score was considerably associated with MSI-L status while higher with microsatellite stability (MSS) status (Fig. 7G). Finally, the correlation analysis between the ANRGs score and tumor cell stemness score demonstrated the ANRGs score to be considerably and positively correlated with RNAss, which indicates more pronounced stem cell characteristics and lower cellular differentiation for tumor cells with higher risk scores.

### 3.8. Comprehensive analysis of ANRGs signature

Based on the analyses of the seven-gene signature that comprised the risk score model and the abundance of immune cells, it has been found that many of these signatures were closely linked to multiple immune cell infiltrations (Fig. 8A). As illustrated in Fig. 8B and C, analyzing the differences in the distribution of somatic mutations among the seven signatures within different ANRGs Score groups revealed that TMB has been highly prevalent in the high-score group, where the most prominent somatic mutation was ITGAV (3%) while the most significant one in the low-risk group was OGT (4%). According to research, genetic mutations and tumor cell heterogeneity affect the sensitivity of tumors to certain drugs. It was also found that there exists a significantly positive correlation between ITGAV expression and the susceptibility of most chemotherapeutic drugs retrieved from the CTRP and GDSC databases (Fig. 8D–E). A single-cell data analysis revealed 11 cell types and 18 cell clusters in the GSE146100 dataset and showed the distribution of various cell types (Fig. 8F) as well as the expression of seven signatures in different cells (Fig. 8G). There was a significant expression

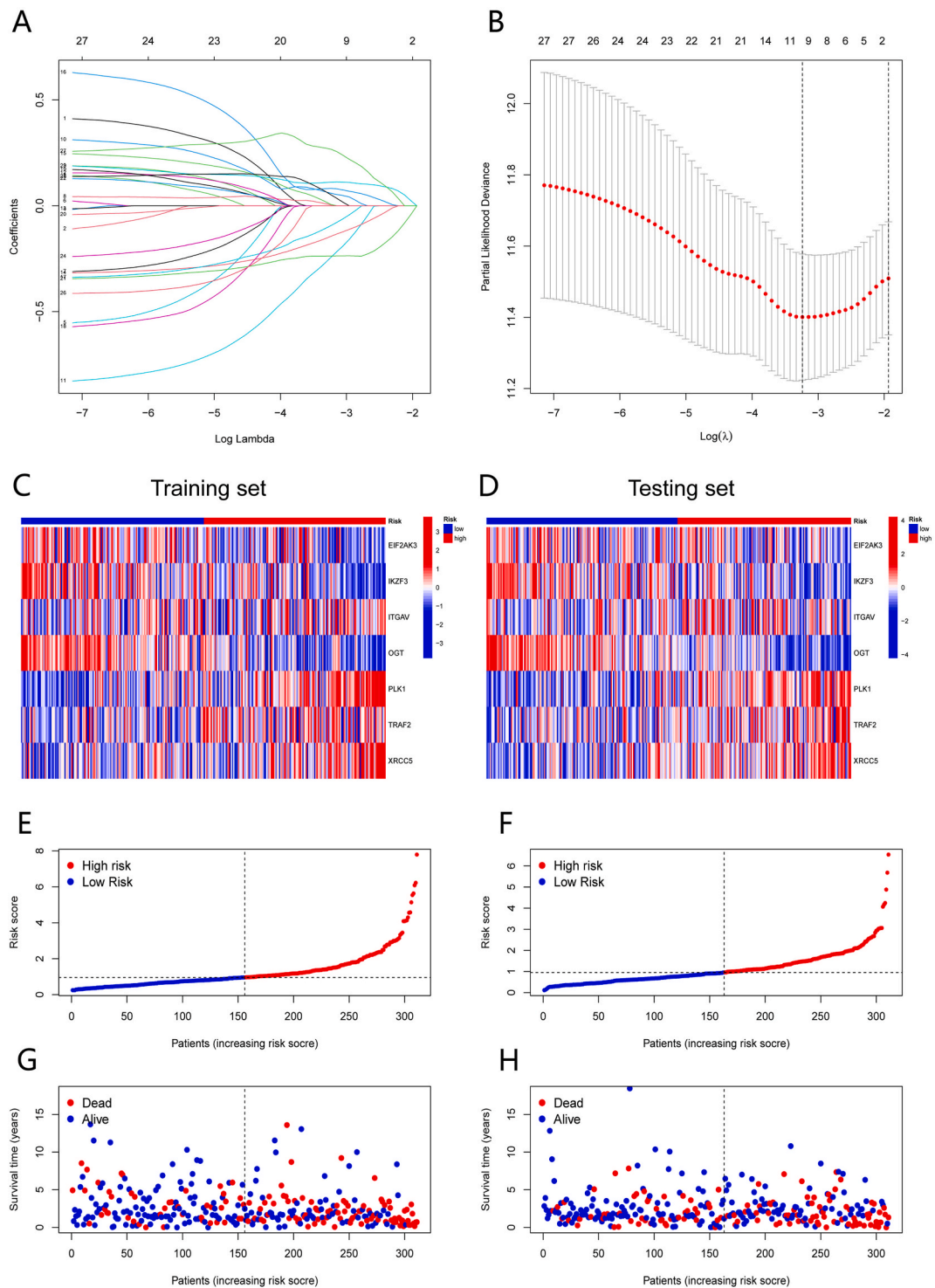
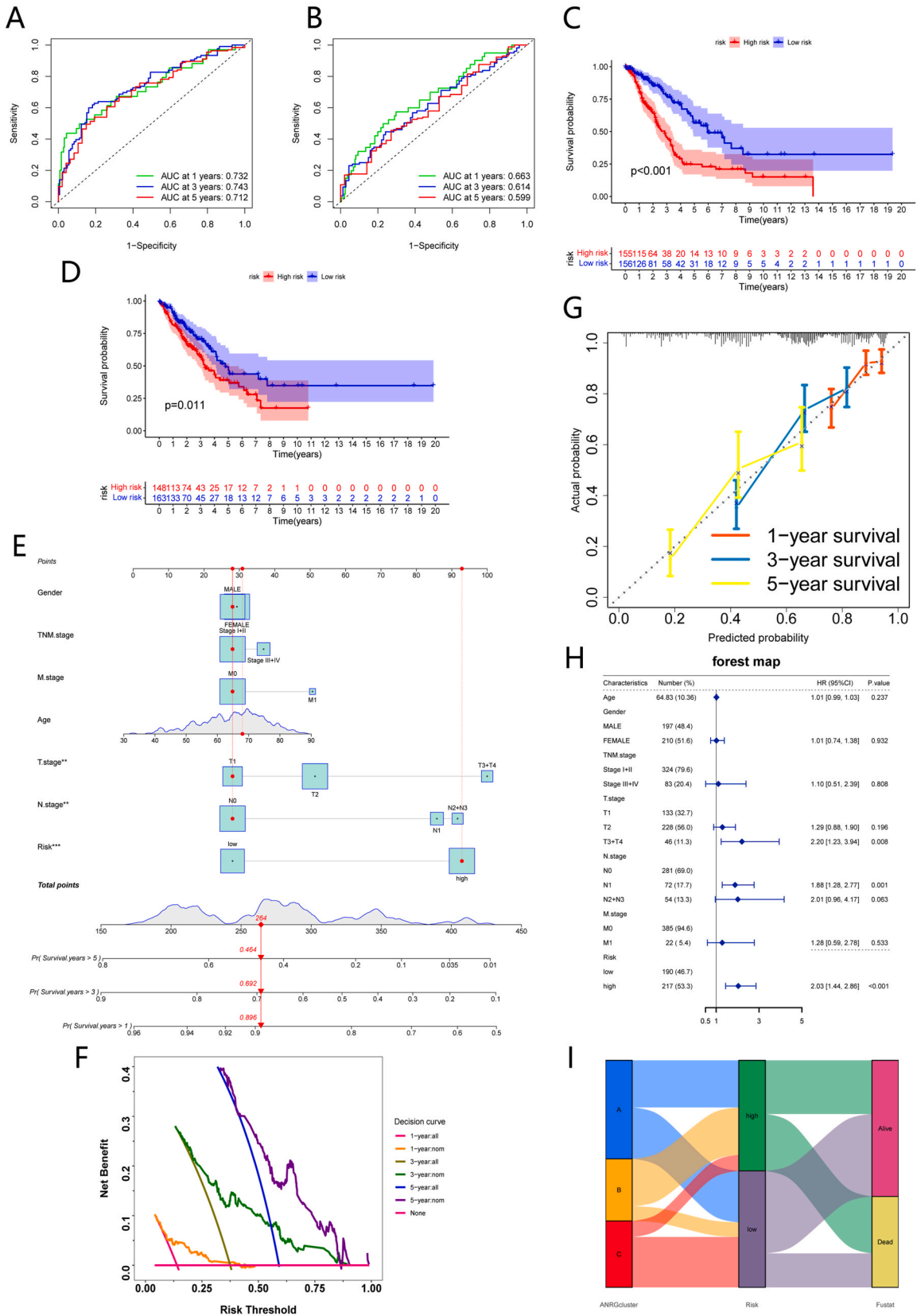


**Fig. 5.** Risk prediction model development based on ANRGs signature. (A) LASSO regression analysis with 10-fold cross-validation establishing a model incorporating ANRGs associated with prognosis. (B) Coefficient profile plots of ANRGs. (C–D) The heat map shows the expression pattern of seven hub ANRGs at different risk groups in training and testing sets. (E–F) Illustration of the ANRGs model based on the risk score of training as well as testing sets. (G–H) Survival time and status in low- as well as high-risk groups for training and testing sets.



(caption on next page)

**Fig. 6.** The clinical value of a nomogram for LUAD patients. (A–B) ROC curves predicting sensitivity as well as specificity for 1-, 3-, and 5-year survival in training and testing sets. (C–D) Survival analysis between high and low-risk subgroups. (E) Nomogram for predicting the RFS of patients based on risk score and clinicopathological factors. (F) DCA curves of the nomogram for OS among LUAD patients. (G) Cumulative curves of nomogram showing the survival probability over time progression. (H) Forest plot presenting multivariable Cox regression analysis of clinical characteristics and risk score. (I) Alluvial diagram of a relationship between subtypes, risk score, and living status.

of IKZF3 in most immune cells, however, ITGAV was more prominent in endothelial, fibroblast, and epithelial cells, while OGT and XRCC5 were detected in all cell types (Fig. 8G). Finally, based on the HPA database, the seven-ANRG signature was verified in terms of their expression levels by immunohistochemistry, and in comparison to normal tissues, they were highly expressed in LUAD tissue (Fig. 9A–G).

#### 4. Discussion

LUAD constitutes more than 40% of non-small cell lung cancers, making it the most prevalent histological type [23]. There are four stages in the advancement of LUAD, starting with atypical adenomatous hyperplasia (AAH), progressing to adenocarcinoma in situ (AIS), minimally invasive adenocarcinoma (MIA), and eventually developing into invasive adenocarcinoma, of which the most common subtype is invasive non-mucinous adenocarcinoma [24]. Despite great progress made in the pathogenesis of adenocarcinoma, LUAD remains one of the most invasive and lethal types of tumors with an overall survival time of low than 5 years [25]. Immunotherapy is an emerging therapeutic approach that includes ICP inhibitors (ICIS), therapeutic antibodies, and cellular therapies [26]. Also, more and more immunosuppressants are receiving approval for clinical use in recent years, but the survival, as well as prognosis of patients, are not improved significantly. Since adenocarcinomas are highly metastatic and heterogeneous, it is imperative to develop gene signatures that identify the potential mechanism of tumor metastasis in guiding treatment and prognosis prediction.

Tsvetkov et al. have reported the correlation between elesclomol-mediated cancer cytotoxicity increased ferritin-1 (FDX1) levels, mitochondrial respiration frequency, and dependent on copper availability [27]. In addition, mitochondrial respiration-dependent cells were more sensitive to elesclomol processing than anaerobic glycolysis-dependent cells [28]. A distinct cell death type known as cuproptosis occurs when intracellular copper accumulates, causing mitochondrial lipid-based proteins aggregation and Fe/S proteins destabilization. Copper can directly bind to lipoproteins and induce abnormal oligomerization and TCA cycle disruption, which may be a key step in cuproptosis [29]. In contrast, elesclomol treatment did not activate caspase-3, a hallmark of apoptosis, and inhibiting the apoptotic pathway or other known PCD pathways could not prevent cuproptosis, indicating that this copper-dependent, mitochondria-induced cell death is distinguished from known cellular death patterns such as apoptosis, necroptosis, or ferroptosis, but its sensitivity mechanisms remain largely unknown.

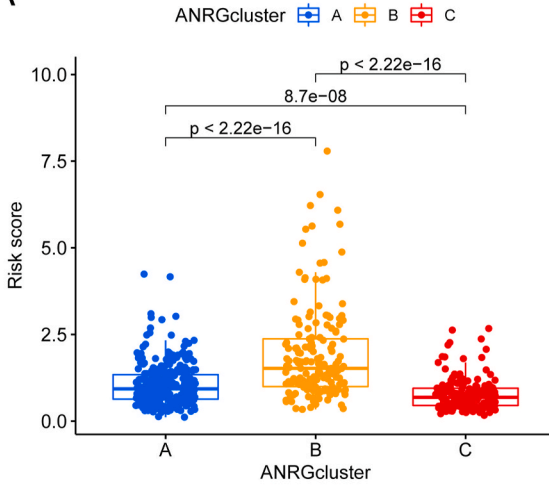
When loss of either cell adhesion or improper adhesion to ECM occurs, normal epithelial cells losing contact with ECM would rapidly undergo apoptosis, which is called anoikis [30]. Anoikis is a specific PCD pathway initiated by the detachment of cells from ECM playing an important role in body development, tissue homeostasis and sickness development [31]. However, the primary characteristic of tumor development is the ability to transform cells in “independent” growth conditions. One of the creatures of invasive cancer cells is their ability to escape anoikis allowing them to survive under adverse metastatic conditions with loss of ECM. This resistance to anoikis turns out to be associated with loss of intracellular environmental homeostasis, cancer growth, and metastasis which has been termed anoikis resistance. Such anoikis-resistant cancer cells possess the ability to spread through the peripheral circulatory system in distant tissues or organs [5]. The investigation of the molecular mechanism of anoikis-resistance will aid in the development of effective therapies for human malignancies.

Although anoikis is a barrier to metastasis, tumor cells tend to acquire stronger resistance to anoikis, thus increasing the potential of metastasis. Whereas copper toxicity is closely related to mitochondrial activity, and mitochondrial oxidative metabolism is a key inhibitor of tumor metastasis, excessive accumulation of copper induces cell death and participates in a key step of the TCA cycle. Some studies have shown that ROS produced by mitochondrial respiration is an inherent by-product of oxidative metabolism [32], which can stimulate glucose oxidation and enhance oxidative stress in cancer cells, restoring cellular susceptibility to anoikis [11]. The joint role of cuproptosis and anoikis in tumor growth and metastasis has not been further investigated. Therefore, a comprehensive analysis of the molecular characteristics of anoikis-related genes (ANRGs) co-expressed with cuproptosis in LUAD is of great significance for the development of precise therapeutic regimens.

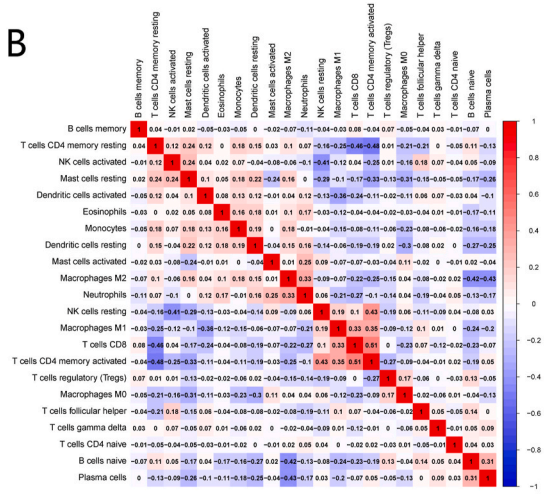
Several studies have demonstrated that ARGs display a vital role in tumor metastasis, invasion and prognosis. According to Miao et al., FOXC2 is capable of promoting the growth, metastasis, and resistance to drugs of ovarian carcinoma cells [33]. In another study, Liu et al. confirmed CRABP2's close association with the migration and invasive ability of thyroid cancer cells with an adverse effect on prognosis [34]. The use of ANRGs as prognostic indicators in LUAD, however, is limited. On the basis of cuproptosis-related genes' expressions, 141 co-expressed anoikis-related genes were identified with further acquisition of 27 ANRGs by differential and survival analyses. Using an unsupervised consistent clustering algorithm, a total of three LUAD subtypes were obtained, which exhibited significant differences in expression and survival. Also, considerable variations in immune cell infiltration were found across these three groups. GSVA enrichment analysis showed that LUAD subtypes were abundant in the cell cycle and oxidative metabolism pathways.

Considering the critical role of anoikis in tumor growth and metastasis, as well as the heterogeneity among different subtypes of LUAD, it is crucial to determine ANRGs' prognostic significance in LUAD patients. Therefore, a quantitative prognosis risk score (ANRGsScore) based on 7 ANRGs has been developed including EIF2AK3, IKZF3, ITGAV, OGT, TRAF2, XRCC5, PLK1. Previous studies

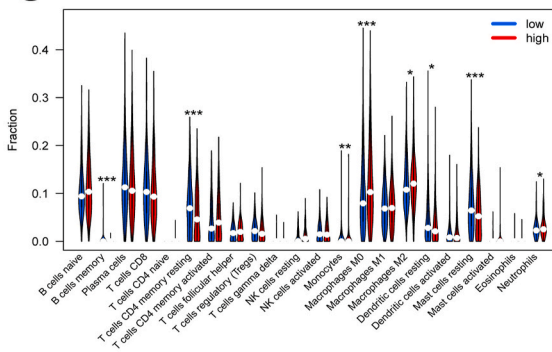
**A**



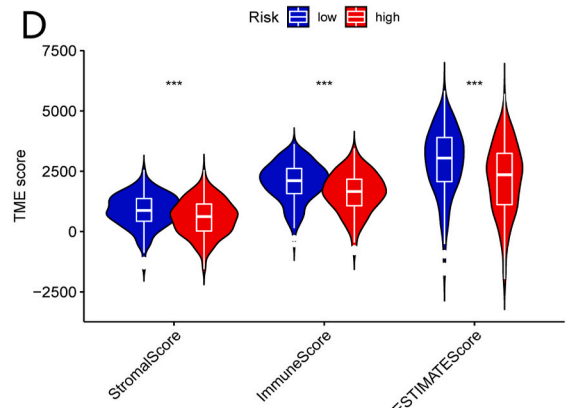
**B**



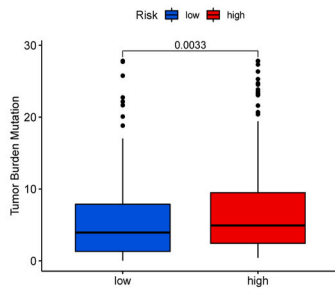
**C**



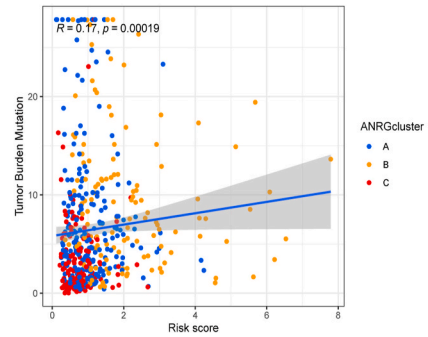
**D**



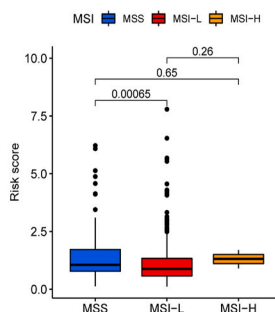
**E**



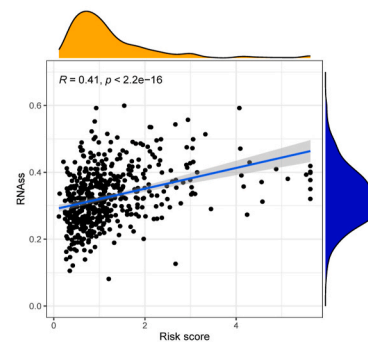
**F**



**G**



**H**



(caption on next page)

**Fig. 7.** Comparison of the tumor microenvironment and mutation properties between subgroups. (A) Differences in ANRGs score between three clusters. (B) The correlation of various TME immune cells. (C) The component percentage of immune infiltrating cells between high- as well as low-risk groups. (D) Correlation between immune and stromal scores in different risk subgroups. (E) Tumor mutation burden (TMB) of different risk score groups. (F) Spearman correlation of TMB and risk score. (G) Correlations between risk score and MSI. (H) Correlations between risk score and CSC index.

confirmed that these gene signatures are closely associated with tumor progression. The ECM regulates cell adhesion and cell attachment, while integrin regulates the location and activity of protein hydrolases during ECM remodeling, promoting tumor invasion and migration [35]. Previous research demonstrated integrin subunit  $\alpha$ -V gene (ITGAV) can promote the occurrence, metastasis, proliferation, invasion, and self-renewal of breast cancer [36]. Furthermore, a positive association between ITGAV expression and chemotherapeutic drug sensitivity was exhibited, which has guiding implications in clinical practice. Alvaro et al., have found that in breast cancer, breast epithelial cells detached from ECM can synergistically induce antioxidant response and autophagy through activation of PERK to reduce the level of ROS to delay anoikis [37–39]. It has also been demonstrated that OGT/O-GlcNAcylation has a high level in many cancers and is closely related to poor survival, unanchored growth, migration, and invasion of lung cancer [40,41]. Anoikis resistance of tumor cells was found to be promoted by TRAF2 interacting with the N-terminus of FAK. Similarly, down-regulation of TRAF2 and FAK was found to increase the susceptibility of human breast cancer cells to anoikis in MDA-MB-231 [42,43]. Most cancer types are accompanied by a decline in genetic integrity and stability, and the key function of XRCC5 is to maintain genomic stability and human ontogeny. A study has demonstrated that XRCC5 alterations were more common in LUAD and played a key role in tumorigenesis [44]. Lin et al., found that NF- $\kappa$ B subunit  $\text{relA}$  could directly bind to the PLK1 promoter and further inhibited the ubiquitination and degradation of b-catenin protein, thus regulating the level of b-catenin protein and protecting esophageal cancer cells from anoikis [45]. Li et al. reported that Aiolos (encoded by IKZF3) reduces the expression of adhesion-related genes, and interferes with cell-matrix interactions, thus blocking the process of anoikis and promoting metastasis [46,47].

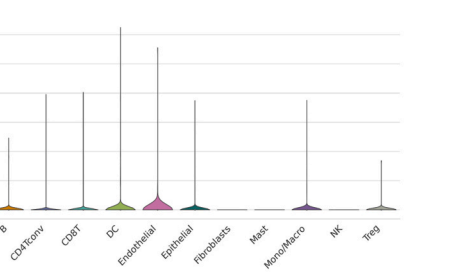
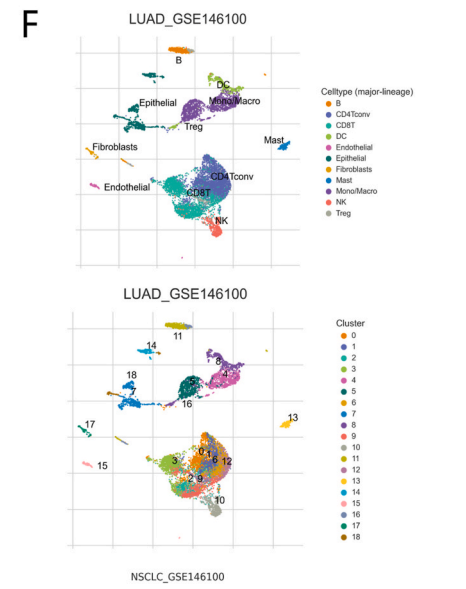
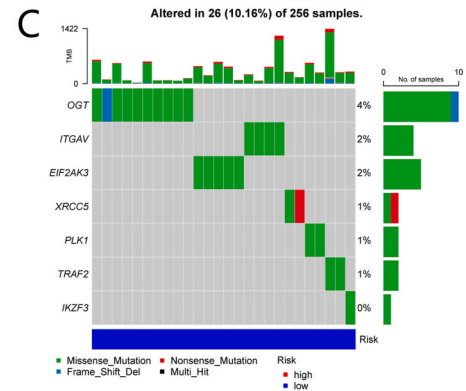
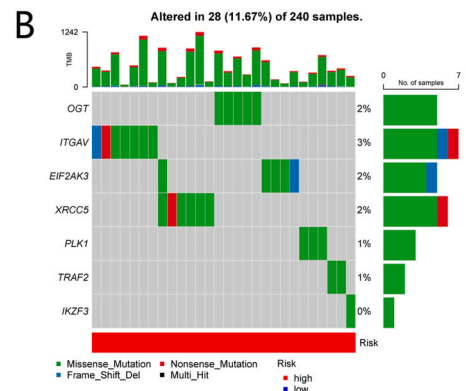
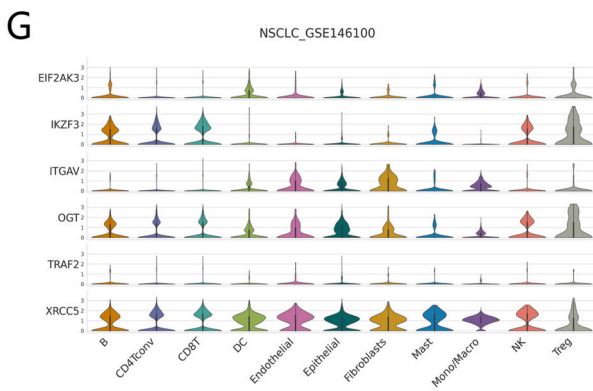
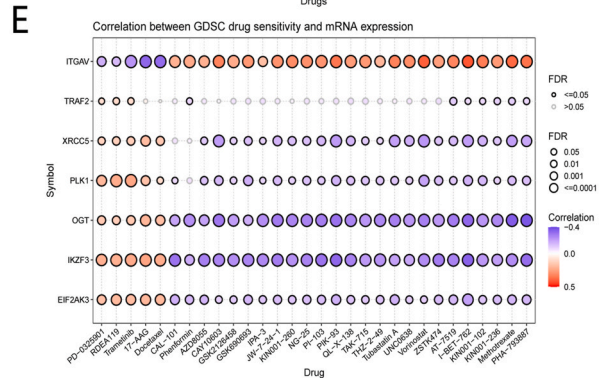
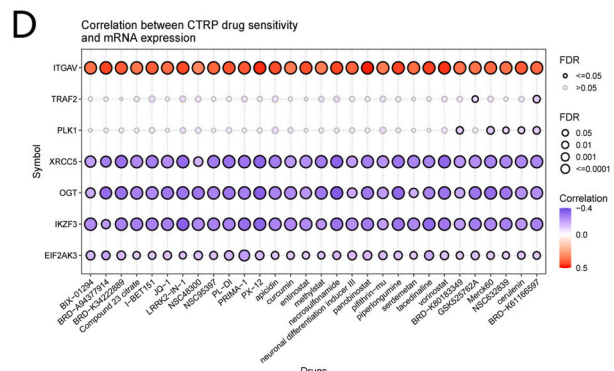
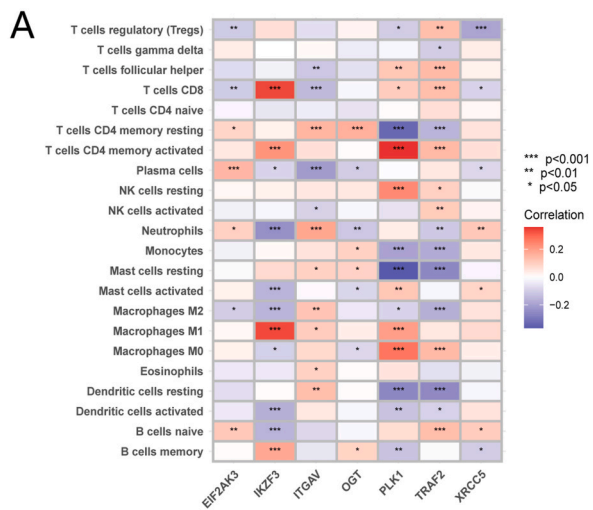
An important factor in tumor growth, metastasis, and therapy is TME, consisting of ECM, mesenchymal cells, tumor vessels, and various immune cells [48]. Initiation of metastasis relies on cross-dialogue between tumor cells and stromal cells, and epithelial-mesenchymal transformation (EMT) is adopted in single cells [49]. We constructed the ANRG risk score to evaluate the change pattern of TME in LUAD patients. Compared with high-risk score, the low-risk group had higher Stromal Score, Immune Score and final ESTIMATE TME Score, which demonstrated that the ANRG risk score could be used to observe the immune infiltration of LUAD and predict the invasion pattern of TME or tumor immunophenotype. In addition, TMB and MSI have been certificated to be associated with tumor proliferation and survival [50]. Tumor cells utilize several mechanisms to maintain survival, including restarting metabolic demand to exploit available resources in a new environment, escaping anoikis upon detachment from ECM, and immunosuppression by inhibiting the activity of immune cells [51]. A significant role played by lung cancer immunotherapy in controlling and clearing cancer cells is to restore the normal anti-tumor immune function of the body by restarting and maintaining the tumor-immune microenvironment [52]. The relationship between seven signatures and different immune cell abundance has been analyzed and their expression in immune cells was verified based on the single-cell database. It has been turned out that these hub genes were closely linked to multiple immune cell infiltrations. According to the results, they might be crucial in predicting immunotherapy's effectiveness.

Further analysis and validation of ANRGs scores in predicting the prognosis of LUAD patients were carried out. The results revealed considerable variations in clinicopathological characteristics, prognosis, mutations, TMB, MSI, and tumor stem cell scores between low- and high-risk groups, indicating that ANRGs score is a reliable index for assessing survival outcomes and tumor treatment effects of patients. Then, the forecast value of the ANRGs score was further improved by integrating it with clinicopathological creatures to establish a quantitative nomogram. This prognostic model may be applied to stratify the prognosis and help individualize the curing of patients.

Although this study has been validated with multiple perspectives and databases, there are still several limitations. First, all samples utilized in the study were retrospective data from public databases, which required further verification by extensive prospective studies. Second, considering the heterogeneity between cells, single-cell sequencing techniques should be applied to reveal genomic differences between cell proportions and phenotypes. Third, although the prognostic nomogram has high predictive accuracy, it fails to include some prominent clinical variables, including surgery, radiotherapy and chemotherapy, and immunotherapy, in the analysis. For calibrating the prediction model, a larger and more detailed sample size could be added. Finally, detailed *in vivo*, as well as *in vitro* experiments, are required for exploring the underlying mechanisms of ANRGs.

## 5. Conclusion

In summary, three subtypes of ANRGs in LUAD have been identified according to TCGA and GEO data. We compared the prognosis status of different subtypes and then established a risk score model based on seven signatures. Further, an analysis of clinical features, immune infiltration, and mutation characteristics on the basis of the risk score has been carried out. Results indicate that ANRGs are valuable prognostic markers that can be utilized to help treat LUAD more accurately.



(caption on next page)

**Fig. 8.** Comprehensive analysis of 7 hub genes. (A) Immune cell relationship with seven hub genes. (B–C) Somatic mutation feature-related waterfall plot for high-as well as low ANRGs scores. (D–E) Bubble chart depicting the relationship between CTRP/GDSC drug sensitivity and seven hub ANRGs. The color transition from blue to red represents the link between CENPI expression and IC50. A positive relationship indicates that high expression of this gene provides resistance to the medication and vice versa. (F) Annotation of all LUAD TME-associated cell types in GSE146100. (G) Expression of EIF2AK3, IKZF3, ITGAV, OGT, TRAF2, XRCC5, and PLK1 in different cells. (For interpretation of the references to color in this figure legend, the reader is referred to the Web version of this article.)

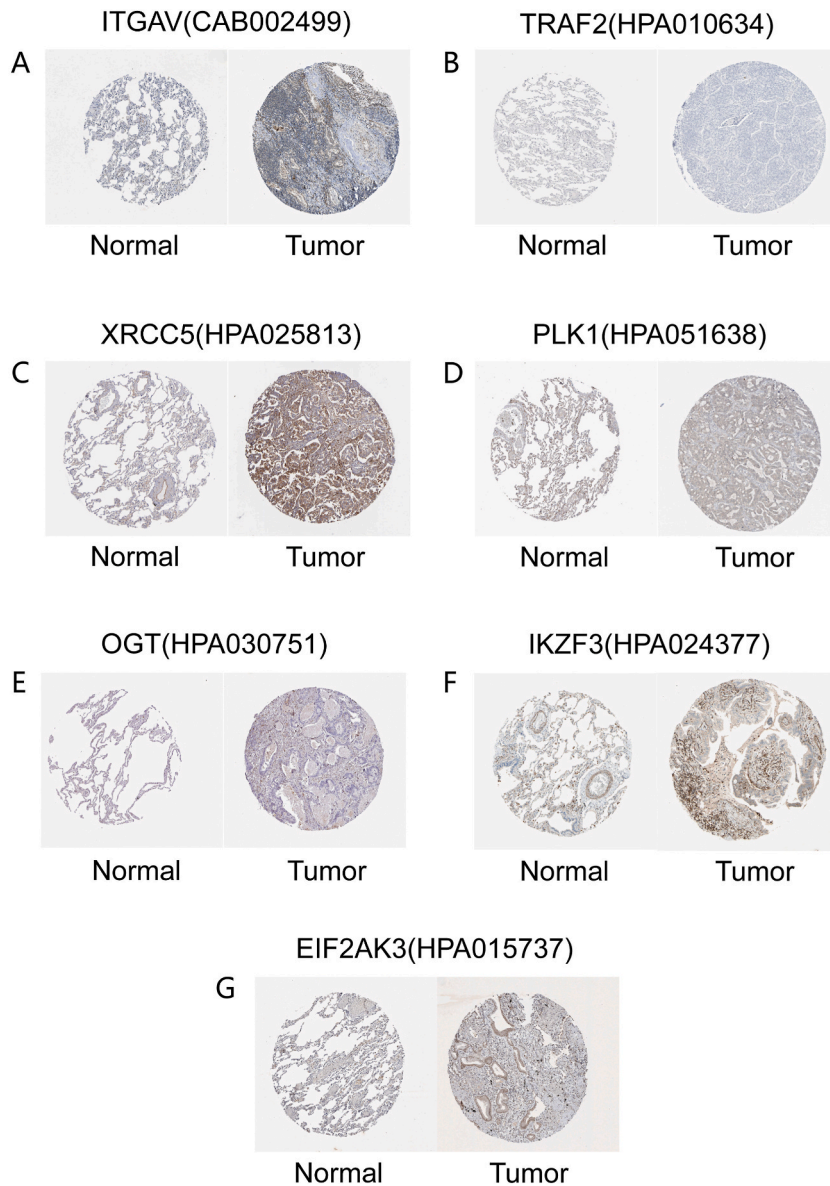


**Fig. 9.** The immunohistochemistry landscape of seven hub genes. (A) ITGAV (CAB002499), (B) TRAF2 (HPA010634), (C) XRCC5 (HPA025813), (D) PLK1 (HPA051638), (E) OGT (HPA030751), (F) IKZF3 (HPA024377) and (G) EIF2AK3 (HPA015737).

#### Author contribution statement

Wenjun Mao; Mingfeng Zheng; Ying Cai; Guanyu Jiang: Conceived and designed the experiments. Guanyu Jiang: Performed the experiments. Guanyu Jiang; Chenghu Song; Xiaokun Wang: Analyzed and interpreted the data. Yongrui Xu; Huixing Li; Zhao He: Contributed reagents, materials, analysis tools or data. Guanyu Jiang; Chenghu Song; Xiaokun Wang: Wrote the paper.

## Funding statement

This work was partially supported by the Natural Science Foundation of Jiangsu Province (BK20210068), the Top Talent Support Program for Young and Middle-aged People of Wuxi Municipal Health Commission (HB2020003), the Mega-project of Wuxi Commission of Health (Z202216) and the High-end Medical Expert Team of the 2019 Taihu Talent Plan (2019-THRCTD-1).

## Data availability statement

The datasets presented in this study can be found in TCGA-LUAD (The Cancer Genome Atlas; <https://portal.gdc.cancer.gov/>), UCSC Xena (<https://xena.ucsc.edu/>), GSE26939 from GEO(Gene Expression Omnibus; <https://www.ncbi.nlm.nih.gov/geo/>) database.

## Ethics statement

We performed secondary analyses on the data from online databases, which is publicly available at an open resource web platform.

## Declaration of competing interest

The authors declare that they have no known competing financial interests or personal relationships that could have appeared to influence the work reported in this paper.

## Acknowledgment

Thanks to all the peer reviewers for their opinions and suggestions. We thank Bullet Edits Limited for the linguistic editing and proofreading of the manuscript.

## Appendix A. Supplementary data

Supplementary data to this article can be found online at <https://doi.org/10.1016/j.heliyon.2023.e14091>.

## References

- [1] R.L. Siegel, K.D. Miller, H.E. Fuchs, A. Jemal, Cancer statistics, 2022, *Ca - Cancer J. Clin.* 72 (2022) 7–33, <https://doi.org/10.3322/caac.21708>.
- [2] R.S. Herbst, D. Morgensztern, C. Boshoff, The biology and management of non-small cell lung cancer, *Nature* 553 (2018) 446–454, <https://doi.org/10.1038/nature25183>.
- [3] O. Rodak, M.D. Peris-Díaz, M. Olbromski, M. Podhorska-Okotów, P. Dzięgiel, Current landscape of non-small cell lung cancer: epidemiology, histological classification, targeted therapies, and immunotherapy, *Cancers* 13 (2021) 4705, <https://doi.org/10.3390/cancers13184705>.
- [4] S.U. Khan, K. Fatima, F. Malik, Understanding the cell survival mechanism of anoikis-resistant cancer cells during different steps of metastasis, *Clin. Exp. Metastasis* (2022), <https://doi.org/10.1007/s10585-022-10172-9>.
- [5] Z. Zhu, C. Fang, H. Xu, L. Yuan, Y. Du, Y. Ni, Y. Xu, A. Shao, A. Zhang, M. Lou, Anoikis resistance in diffuse glioma: the potential therapeutic targets in the future, *Front. Oncol.* 12 (2022), 976557, <https://doi.org/10.3389/fonc.2022.976557>.
- [6] P.A. Cobine, D.C. Brady, Cuproptosis: cellular and molecular mechanisms underlying copper-induced cell death, *Mol. Cell.* 82 (2022) 1786–1787, <https://doi.org/10.1016/j.molcel.2022.05.001>.
- [7] P. Tsvetkov, S. Coy, B. Petrova, M. Dreishpoon, A. Verma, M. Abdusamad, J. Rossen, L. Joesch-Cohen, R. Humeidi, R.D. Spangler, J.K. Eaton, E. Frenkel, M. Kocak, S.M. Corsello, S. Lutsenko, N. Kanarek, S. Santagata, T.R. Golub, Copper induces cell death by targeting lipoylated TCA cycle proteins, *Science* 375 (2022) 1254–1261, <https://doi.org/10.1126/science.abf0529>.
- [8] P. Lelièvre, L. Sancey, J.-L. Coll, A. Deniaud, B. Busser, The multifaceted roles of copper in cancer: a trace metal element with dysregulated metabolism, but also a target or a bullet for therapy, *Cancers* 12 (2020) 3594, <https://doi.org/10.3390/cancers12123594>.
- [9] Y. Wang, L. Zhang, F. Zhou, Cuproptosis: a new form of programmed cell death, *Cell. Mol. Immunol.* 19 (2022) 867–868, <https://doi.org/10.1038/s41423-022-00866-1>.
- [10] M. Benhar, D. Engelberg, A. Levitzki, ROS, stress-activated kinases and stress signaling in cancer, *EMBO Rep.* 3 (2002) 420–425, <https://doi.org/10.1093/embo-reports/kvf094>.
- [11] J. Lu, M. Tan, Q. Cai, The Warburg effect in tumor progression: mitochondrial oxidative metabolism as an anti-metastasis mechanism, *Cancer Lett.* 356 (2015) 156–164, <https://doi.org/10.1016/j.canlet.2014.04.001>.
- [12] M. Hanifeh, F. Atefi, XIAP as a multifaceted molecule in Cellular Signaling, *Apoptosis* 27 (2022) 441–453, <https://doi.org/10.1007/s10495-022-01734-z>.
- [13] F. Aoudjit, K. Vuori, Matrix attachment regulates Fas-induced apoptosis in endothelial cells: a role for c-flip and implications for anoikis, *J. Cell Biol.* 152 (2001) 633–643, <https://doi.org/10.1083/jcb.152.3.633>.
- [14] P. Kumar, A. Yadav, S.N. Patel, M. Islam, Q. Pan, S.D. Merajver, T.N. Teknos, Tetrathiomolybdate inhibits head and neck cancer metastasis by decreasing tumor cell motility, invasiveness and by promoting tumor cell anoikis, *Mol. Cancer* 9 (2010) 206, <https://doi.org/10.1186/1476-4598-9-206>.
- [15] M.J. Goldman, B. Craft, M. Hastie, K. Repecka, F. McDade, A. Kamath, A. Banerjee, Y. Luo, D. Rogers, A.N. Brooks, J. Zhu, D. Haussler, Visualizing and interpreting cancer genomics data via the Xena platform, *Nat. Biotechnol.* 38 (2020) 675–678, <https://doi.org/10.1038/s41587-020-0546-8>.
- [16] A.D. Rouillard, G.W. Gundersen, N.F. Fernandez, Z. Wang, C.D. Monteiro, M.G. McDermott, A. Ma'ayan, The Harmonizome: a Collection of Processed Datasets Gathered to Serve and Mine Knowledge about Genes and Proteins (2016) baw100, Database (Oxford), 2016, <https://doi.org/10.1093/database/baw100>.
- [17] P. Bardou, J. Mariette, F. Escudié, C. Djemiel, C. Klopp, jvenn: an interactive Venn diagram viewer, *BMC Bioinf.* 15 (2014) 293, <https://doi.org/10.1186/1471-2105-15-293>.
- [18] D. Szklarczyk, A.L. Gable, K.C. Nastou, D. Lyon, R. Kirsch, S. Pyysalo, N.T. Doncheva, M. Legeay, T. Fang, P. Bork, L.J. Jensen, C. von Mering, The STRING database in 2021: customizable protein-protein networks, and functional characterization of user-uploaded gene/measurement sets, *Nucleic Acids Res.* 49 (2021) D605–D612, <https://doi.org/10.1093/nar/gkaa1074>.

- [19] H. Mi, A. Muruganujan, D. Ebert, X. Huang, P.D. Thomas, PANTHER version 14: more genomes, a new PANTHER GO-slim and improvements in enrichment analysis tools, *Nucleic Acids Res.* 47 (2019) D419–D426, <https://doi.org/10.1093/nar/gky1038>.
- [20] M. Kanehisa, M. Furumichi, M. Tanabe, Y. Sato, K. Morishima, KEGG: new perspectives on genomes, pathways, diseases and drugs, *Nucleic Acids Res.* 45 (2017) D353–D361, <https://doi.org/10.1093/nar/gkw1092>.
- [21] C.-J. Liu, F.-F. Hu, M.-X. Xia, L. Han, Q. Zhang, A.-Y. Guo, GSCALite: a web server for gene set cancer analysis, *Bioinformatics* 34 (2018) 3771–3772, <https://doi.org/10.1093/bioinformatics/bty411>.
- [22] D. Sun, J. Wang, Y. Han, X. Dong, J. Ge, R. Zheng, X. Shi, B. Wang, Z. Li, P. Ren, L. Sun, Y. Yan, P. Zhang, F. Zhang, T. Li, C. Wang, TISCH: a comprehensive web resource enabling interactive single-cell transcriptome visualization of tumor microenvironment, *Nucleic Acids Res.* 49 (2021) D1420–D1430, <https://doi.org/10.1093/nar/gkaa1020>.
- [23] G. Lambe, M. Durand, A. Buckley, S. Nicholson, R. McDermott, Adenocarcinoma of the lung: from BAC to the future, *Insights Imaging* 11 (2020) 69, <https://doi.org/10.1186/s13244-020-00875-6>.
- [24] L. Succony, D.M. Rassl, A.P. Barker, F.M. McCaughan, R.C. Rintoul, Adenocarcinoma spectrum lesions of the lung: detection, pathology and treatment strategies, *Cancer Treat Rev.* 99 (2021), 102237, <https://doi.org/10.1016/j.ctrv.2021.102237>.
- [25] T.V. Denisenko, I.N. Budkevich, B. Zhivotovskiy, Cell death-based treatment of lung adenocarcinoma, *Cell Death Dis.* 9 (2018) 117, <https://doi.org/10.1038/s41419-017-0063-y>.
- [26] S. Hammerschmidt, H. Wirtz, Lung cancer: current diagnosis and treatment, *Dtsch Arztebl Int* 106 (2009) 809–818, <https://doi.org/10.3238/arztebl.2009.0809>, quiz 819–820.
- [27] W.-J. Duan, R.-R. He, Cuproptosis: copper-induced regulated cell death, *Sci. China Life Sci.* 65 (2022) 1680–1682, <https://doi.org/10.1007/s11427-022-2106-6>.
- [28] D. Tang, X. Chen, G. Kroemer, Cuproptosis: a copper-triggered modality of mitochondrial cell death, *Cell Res.* 32 (2022) 417–418, <https://doi.org/10.1038/s41422-022-00653-7>.
- [29] S.-R. Li, L.-L. Bu, L. Cai, Cuproptosis: lipoylated TCA cycle proteins-mediated novel cell death pathway, *Signal Transduct. Targeted Ther.* 7 (2022) 158, <https://doi.org/10.1038/s41392-022-01014-x>.
- [30] H. Hji, S. Jy, K. Sh, Y. Uj, K. H, J. Ej, Y. He, H. Ek, G. Sh, M. A, L. Js, Y. Sk, S. J, K. Yn, Fibronectin regulates anoikis resistance via cell aggregate formation, *Cancer Lett.* 508 (2021), <https://doi.org/10.1016/j.canlet.2021.03.011>.
- [31] J. Wang, Z. Luo, L. Lin, X. Sui, L. Yu, C. Xu, R. Zhang, Z. Zhao, Q. Zhu, B. An, Q. Wang, B. Chen, E.L.-H. Leung, Q. Wu, Anoikis-associated lung cancer metastasis: mechanisms and therapies, *Cancers* 14 (2022) 4791, <https://doi.org/10.3390/cancers14194791>.
- [32] F.A. Urra, S. Fuentes-Retamal, C. Palominos, Y.A. Rodríguez-Lucart, C. López-Torres, R. Araya-Maturana, Extracellular matrix signals as drivers of mitochondrial bioenergetics and metabolic plasticity of cancer cells during metastasis, *Front. Cell Dev. Biol.* 9 (2021), 751301, <https://doi.org/10.3389/fcell.2021.751301>.
- [33] M.S. Recouvreux, J. Miao, M.C. Gozo, J. Wu, A.E. Walts, B.Y. Karlan, S. Orsulic, FOXC2 promotes vasculogenic mimicry in ovarian cancer, *Cancers* 14 (2022) 4851, <https://doi.org/10.3390/cancers14194851>.
- [34] C.-L. Liu, Y.-C. Hsu, C.-Y. Kuo, J.-Y. Jhuang, Y.-S. Li, S.-P. Cheng, CRABP2 is associated with thyroid cancer recurrence and promotes invasion via the integrin/FAK/AKT pathway, *Endocrinology* (2022), <https://doi.org/10.1210/endo/bqac171> bqac171.
- [35] F.O. Adeshakin, A.O. Adeshakin, L.O. Afolabi, D. Yan, G. Zhang, X. Wan, Mechanisms for modulating anoikis resistance in cancer and the relevance of metabolic reprogramming, *Front. Oncol.* 11 (2021), 626577, <https://doi.org/10.3389/fonc.2021.626577>.
- [36] I.W.-Y. Cheuk, M.T. Siu, J.C.-W. Ho, J. Chen, V.Y. Shin, A. Kwong, ITGAV targeting as a therapeutic approach for treatment of metastatic breast cancer, *Am J Cancer Res* 10 (2020) 211–223.
- [37] A. Avivar-Valderas, E. Salas, E. Bobrovnikova-Marjon, J.A. Diehl, C. Nagi, J. Debnath, J.A. Aguirre-Ghiso, PERK integrates autophagy and oxidative stress responses to promote survival during extracellular matrix detachment, *Mol. Cell Biol.* 31 (2011) 3616–3629, <https://doi.org/10.1128/MCB.05164-11>.
- [38] M. Yu, J. Lun, H. Zhang, L. Wang, G. Zhang, H. Zhang, J. Fang, Targeting UPR branches, a potential strategy for enhancing efficacy of cancer chemotherapy, *Acta Biochim. Biophys. Sin.* 53 (2021) 1417–1427, <https://doi.org/10.1093/abbs/gmab131>.
- [39] P. Paoli, E. Giannoni, P. Chiarugi, Anoikis molecular pathways and its role in cancer progression, *Biochim. Biophys. Acta* 1833 (2013) 3481–3498, <https://doi.org/10.1016/j.bbamer.2013.06.026>.
- [40] D. Wu, J. Jin, Z. Qiu, D. Liu, H. Luo, Functional analysis of O-GlcNAcylation in cancer metastasis, *Front. Oncol.* 10 (2020), 585288, <https://doi.org/10.3389/fonc.2020.585288>.
- [41] L. Ciraku, E.M. Esquea, M.J. Reginato, O-GlcNAcylation regulation of cellular signaling in cancer, *Cell. Signal.* 90 (2022), 110201, <https://doi.org/10.1016/j.cellsig.2021.110201>.
- [42] D. Siegmund, J. Wagner, H. Wajant, TNF receptor associated factor 2 (TRAF2) signaling in cancer, *Cancers* 14 (2022) 4055, <https://doi.org/10.3390/cancers14164055>.
- [43] S.D. da Silva, B. Xu, M. Maschietto, F.A. Marchi, M.I. Alkailani, K. Bijian, D. Xiao, M.A. Alaoui-Jamali, TRAF2 cooperates with focal adhesion signaling to regulate cancer cell susceptibility to anoikis, *Mol. Cancer Therapeut.* 18 (2019) 139–146, <https://doi.org/10.1158/1535-7163.MCT-17-1261>.
- [44] D.-T. Bau, C.-W. Tsai, C.-N. Wu, Role of the XRC5/XRC6 dimer in carcinogenesis and pharmacogenomics, *Pharmacogenomics* 12 (2011) 515–534, <https://doi.org/10.2217/pgs.10.209>.
- [45] D.-C. Lin, Y. Zhang, Q.-J. Pan, H. Yang, Z.-Z. Shi, Z.-H. Xie, B.-S. Wang, J.-J. Hao, T.-T. Zhang, X. Xu, Q.-M. Zhan, M.-R. Wang, PLK1 is transcriptionally activated by NF- $\kappa$ B during cell detachment and enhances anoikis resistance through inhibiting  $\beta$ -catenin degradation in esophageal squamous cell carcinoma, *Clin. Cancer Res.* 17 (2011) 4285–4295, <https://doi.org/10.1158/1078-0432.CCR-10-3236>.
- [46] X. Li, Z. Xu, W. Du, Z. Zhang, Y. Wei, H. Wang, Z. Zhu, L. Qin, L. Wang, Q. Niu, X. Zhao, L. Girard, Y. Gong, Z. Ma, B. Sun, Z. Yao, J.D. Minna, L.S. Terada, Z. Liu, Aiols promotes anchorage independence by silencing p66Shc transcription in cancer cells, *Cancer Cell* 25 (2014) 575–589, <https://doi.org/10.1016/j.ccr.2014.03.020>.
- [47] L.S. Terada, Z. Liu, Aiols and lymphocyte mimicry in lung cancer, *Mol Cell Oncol* 1 (2014), e29912, <https://doi.org/10.4161/mco.29912>.
- [48] P. Hernández-Camarero, E. López-Ruiz, J.A. Marchal, M. Perán, Cancer: a mirrored room between tumor bulk and tumor microenvironment, *J. Exp. Clin. Cancer Res.* 40 (2021) 217, <https://doi.org/10.1186/s13046-021-02022-5>.
- [49] F. Jiang, Y. Hu, X. Liu, M. Wang, C. Wu, Methylation pattern mediated by m6A regulator and tumor microenvironment invasion in lung adenocarcinoma, 2022, *Oxid. Med. Cell. Longev.* (2022), 2930310, <https://doi.org/10.1155/2022/2930310>.
- [50] C.-R. Guo, Y. Mao, F. Jiang, C.-X. Juan, G.-P. Zhou, N. Li, Computational detection of a genome instability-derived lncRNA signature for predicting the clinical outcome of lung adenocarcinoma, *Cancer Med.* 11 (2022) 864–879, <https://doi.org/10.1002/cam4.4471>.
- [51] J. Majidpoor, K. Mortezaee, Steps in metastasis: an updated review, *Med. Oncol.* 38 (2021) 3, <https://doi.org/10.1007/s12032-020-01447-w>.
- [52] R. Santana-Davila, Chemo and immuno-therapeutic options for non-small cell lung cancer lung cancer, *Surg. Clin.* 102 (2022) 493–498, <https://doi.org/10.1016/j.suc.2022.02.005>.